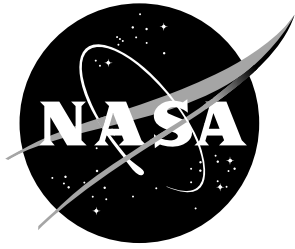


NASA/TM-20230013028



# Partition Thickness Considerations for Additively Manufactured Acoustic Liners

*Michael G. Jones and Douglas M. Nark  
Langley Research Center, Hampton, Virginia*

---

October 2023

## NASA STI Program Report Series

Since its founding, NASA has been dedicated to the advancement of aeronautics and space science. The NASA scientific and technical information (STI) program plays a key part in helping NASA maintain this important role.

The NASA STI program operates under the auspices of the Agency Chief Information Officer. It collects, organizes, provides for archiving, and disseminates NASA's STI. The NASA STI program provides access to the NTRS Registered and its public interface, the NASA Technical Reports Server, thus providing one of the largest collections of aeronautical and space science STI in the world. Results are published in both non-NASA channels and by NASA in the NASA STI Report Series, which includes the following report types:

- **TECHNICAL PUBLICATION.** Reports of completed research or a major significant phase of research that present the results of NASA Programs and include extensive data or theoretical analysis. Includes compilations of significant scientific and technical data and information deemed to be of continuing reference value. NASA counterpart of peer-reviewed formal professional papers but has less stringent limitations on manuscript length and extent of graphic presentations.
- **TECHNICAL MEMORANDUM.** Scientific and technical findings that are preliminary or of specialized interest, e.g., quick release reports, working papers, and bibliographies that contain minimal annotation. Does not contain extensive analysis.
- **CONTRACTOR REPORT.** Scientific and technical findings by NASA-sponsored contractors and grantees.
- **CONFERENCE PUBLICATION.** Collected papers from scientific and technical conferences, symposia, seminars, or other meetings sponsored or co-sponsored by NASA.
- **SPECIAL PUBLICATION.** Scientific, technical, or historical information from NASA programs, projects, and missions, often concerned with subjects having substantial public interest.
- **TECHNICAL TRANSLATION.** English-language translations of foreign scientific and technical material pertinent to NASA's mission.

Specialized services also include organizing and publishing research results, distributing specialized research announcements and feeds, providing information desk and personal search support, and enabling data exchange services.

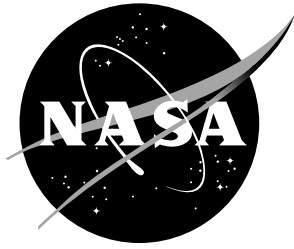
For more information about the NASA STI program, see the following:

- Access the NASA STI program home page at <http://www.sti.nasa.gov>

- Help desk contact information:

<https://www.sti.nasa.gov/sti-contact-form/>  
and select the "General" help request type.

NASA/TM-20230013028



# Partition Thickness Considerations for Additively Manufactured Acoustic Liners

*Michael G. Jones and Douglas M. Nark  
Langley Research Center, Hampton, Virginia*

National Aeronautics and  
Space Administration

Langley Research Center  
Hampton, Virginia 23681-2199

---

October 2023

## Acknowledgments

The authors would like to express their appreciation for the support of the NASA Langley Liner Technology Facility staff in the acquisition of the test data. This work was funded by the Advanced Air Transport Technology Project of the NASA Advanced Air Vehicles Program.

The use of trademarks or names of manufacturers in this report is for accurate reporting and does not constitute an official endorsement, either expressed or implied, of such products or manufacturers by the National Aeronautics and Space Administration.

Available from:

NASA STI Program / Mail Stop 148  
NASA Langley Research Center  
Hampton, VA 23681-2199  
Fax: 757-864-6500

## Abstract

Three types of uniform-depth liners are evaluated to explore the effects of partition thickness on the surface impedance achieved with additively manufactured liners. A transmission line code is used to predict the effects of sound transmission through empty chambers and wire mesh facesheets, and is combined with the Motsinger and Kraft model to account for sound transmission through perforated facesheets. The inclusion of partitions causes a blockage effect, i.e., a portion of the surface is ‘blocked’ (nonactive surface). For liners with no facesheet, these blockage effects are incorporated simply by accounting for the change in cross sectional area between the individual chamber and the unit cell that includes half of a partition thickness around the perimeter of this chamber. Comparison of impedances predicted in this manner with data acquired in the NASA Langley Normal Incidence Tube (NIT) confirms the efficacy of this modeling approach. Two approaches are considered to account for the inclusion of a wiremesh or perforated plate facesheet on these same cores. The first accounts for the effects of partition thickness before including the transfer impedance across the facesheet, while the second reverses these steps. A comparison of data acquired in the NASA NIT with modeled impedances suggests the first approach is best when the facesheet is a wire mesh, but the second approach is preferred when a perforated plate facesheet is used. It is hypothesized that this is due to the fact that a lumped element model is used to compute the transfer impedance across a wire mesh, while the corresponding transfer impedance across a perforated sheet explicitly incorporates the effects of the liner core. However, comparisons of data acquired in the NASA Langley Grazing Flow Impedance Tube with modeled impedances seem slightly better when the first approach is employed with a perforated plate facesheet. Thus, the effects of partition thickness on liners with perforated sheets subjected to grazing incidence sound require further review.

<b>Symbols</b>	<b>Description</b>
$a$	empirical constant (= 64)
$A_a, A_t$	cross-sectional areas for active chamber and total unit cell
$C_D, P_n$	discharge coefficient, Prandtl number
$d, t, t_p$	hole diameter, sheet thickness, partition thickness
$k$	freespace wavenumber
$h, l_s$	core height, chamber side length
$J_0, J_2$	zero- and second-order Bessel functions
$M_{C/L}, \delta_1$	centerline Mach number, boundary layer displacement thickness
$s, d_c$	shear wave number, channel (chamber or orifice) diameter
$v_{\text{rms}}$	rms acoustic particle velocity
$\theta_{\text{gf}}, \theta_f$	acoustic resistance due to grazing flow, normalized DC flow resistance
$\zeta, \theta, \chi$	normalized liner acoustic impedance, resistance, and reactance
$\kappa_i, \kappa_e$	entrance and exit end effect empirical constants; assume $\kappa_i + \kappa_e = 1$
$\rho, c, \mu$	ambient density, sound speed, viscosity
$\sigma, \omega$	perforated facesheet open area ratio, angular frequency
<b>Subscripts</b>	
$a, t$	active, total
$n_{\text{bf}}$	station ‘n’: include blockage effects prior to facesheet effects
$n_{\text{fb}}$	station ‘n’: include facesheet effects prior to blockage effects

# 1 Introduction

As air travel continues to grow, the corresponding increase in noise generated by commercial subsonic turbofan aircraft is of particular concern for neighborhoods surrounding airports. One of the major contributors to this noise is that produced by the fan. Much effort has been placed on reducing the amount of fan noise that is generated, whether by optimizing the sweep and lean of the fan exit guide vanes or by adjusting the distance between the fan and these vanes. Another option is to absorb the sound along the path between the source and the surrounding community. This is achieved by mounting acoustic liners in the walls of the nacelle (see Fig. 1), both upstream (inlet) and downstream (aft bypass duct) of the fan. Modern aircraft employ both options.

Acoustic liners employed in current aircraft typically consist of a honeycomb core sandwiched between a perforated facesheet and a rigid backplate (Fig. 2a). The individual chambers of such a liner behave as Helmholtz resonators, where the peak sound absorption occurs at frequencies for which the quarter-wavelength is approximately equal to the depth of the honeycomb core. This type of liner provides good noise reduction over approximately one octave. When noise reduction is needed over a wider frequency range, it is common to embed a septum (either another perforated sheet or a wire mesh) within the honeycomb core (Fig. 2b). If designed properly, the resultant two-degree-of-freedom liner will provide good noise reduction over two octaves.

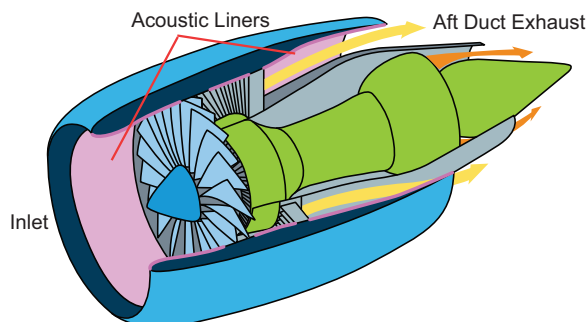


Figure 1: Cutaway drawing of aircraft engine nacelle [Source: NASA].

Although there are many parameters to consider in the liner design process, there are two that are dominant. The first is the amount of treatment surface (i.e., locations where liners can be placed). The second is the ratio of the liner axial length to the height of the flow path. An increase in either the treatment surface or the length-to-height ratio results in improved noise reduction, i.e., less noise radiated from the nacelle.

Recent trends in aircraft design have affected both of these parameters. Aircraft engine nacelles continue to increase in diameter to achieve higher bypass ratios, but this is usually combined with reductions in length and thickness of the nacelle to keep the overall weight within acceptable limits. As a result, the overall surface area is often reduced, sometimes significantly. The increase in diameter also causes the blade passage frequency, a key contributor to tonal fan noise, to be reduced.

A conventional liner would need increased depth to target this lower frequency, but the reduced wall thickness precludes this option.

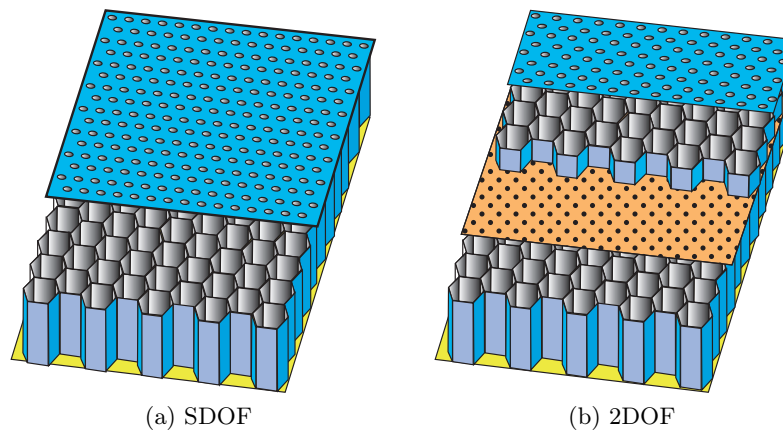


Figure 2: Conventional single- (SDOF) and two-degree-of-freedom (2DOF) liners [Source: NASA].

In response to these issues, there has been significant research directed toward novel acoustic liner designs. Some have targeted the use of conventional materials and manufacturing processes, but many more have focused on the use of additive manufacturing (AM). To date, AM acoustic liners have been limited to laboratory usage, where concepts can be evaluated quickly to determine whether they can be used to achieve desired acoustic properties. As AM materials and processes mature, liners constructed in this manner are expected to transition to use on commercial aircraft.

This paper provides some practical considerations associated with the design and evaluation of novel AM acoustic liners. Whereas conventional liners contain honeycomb core with partitions (walls) that are very thin (typically  $< 0.01''$ ), AM liners often require partitions that are much thicker due to material and manufacturing constraints. Traditional acoustic liner prediction models were originally designed for use with conventional (thin wall) honeycomb core, and must be adjusted to properly account for an increase in partition thickness. This paper examines the effects of partition thickness on the acoustic performance of uniform-depth liners, and offers insight regarding how these effects should be incorporated into the modeling process. This updated modeling process is expected to enable improved liner designs that incorporate more complex core geometries (e.g., variable depth with bent chambers).

The remainder of this paper is organized as follows. Section 2 provides a description of the experimental methods used in this investigation. This includes descriptions of the test rigs, test conditions, and acoustic liners used in this study. Section 3 describes the model used to compute the surface impedance for the first liner type (uniform core, no facesheet). Results are included to validate the modeling approach. Section 4 builds on this result to compute the surface impedance for the second liner type (uniform core, wire mesh facesheet). Two approaches are considered for this computation and comparisons with measured data are used to determine the preferred modeling approach. Section 5 builds on the results from Section 3 to compute the surface impedance for the third liner type (uniform core, perforated facesheet). Again, results from two modeling approaches are compared against measured data to determine the preferred modeling approach.

Finally, Section 6 summarizes conclusions regarding incorporation of partition thickness effects into current modeling practice.

## 2 Experimental Methods

The NASA Langley Normal Incidence Tube (NIT, Fig. 3) and Grazing Flow Impedance Tube (GFIT, Fig. 4) were used to acquire the current data. The NIT is a 2"×2"×36" waveguide with six acoustic drivers. The test liner is placed at the end of the waveguide such that the plane-wave sound field impinges on the liner surface. Two microphones are used with the Two-Microphone Method [1–3] to determine the surface acoustic impedance of the test liner. A controlled-amplitude, swept-sine source [4] allows the sound pressure level (SPL) at the liner surface to be maintained to within  $\pm 0.5$  dB of the target while the frequency is swept through the range of interest (0.4 to 3.0 kHz).

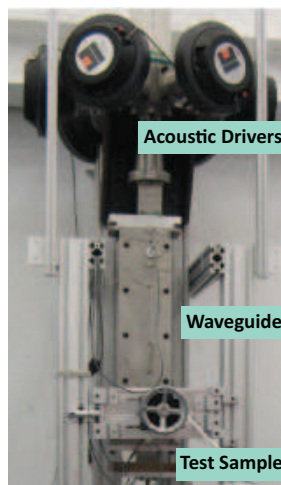


Figure 3: NASA Langley Normal Incidence Tube [Source: NASA].

The GFIT is a 2.0"×2.5"×245" waveguide with twelve acoustic drivers upstream (exhaust mode) and six acoustic drivers downstream (inlet mode) of the test window. Exhaust mode data are used for the current investigation. The surface of the test liner forms a portion of the upper wall of the flow duct. Data acquired with twelve microphones flush-mounted in the lower wall (opposite the liner) are used with the Prony Method [5,6] to educe the impedance of the test liner. A controlled-amplitude, swept-sine source allows the SPL at the liner leading edge to be maintained to within  $\pm 0.5$  dB of the target while the frequency is swept through the range of interest (0.4 to 3.0 kHz). Data were acquired at mean flow Mach numbers of 0.0, 0.3, and 0.5, but only the no flow results are discussed in the current paper. The effects of adding flow will be the focus of a future investigation.

Three sets of samples are used in this study, two for the NIT and one for the GFIT. The first NIT set is used to evaluate the effects of partition thickness on the impedance spectra educed for samples with no facesheet. It is also used to evaluate the effects of adding a wire mesh facesheet. Two sets of samples (NIT Set 2 and GFIT Set 1) are used to evaluate partition thickness effects on the impedance spectra educed when a perforated facesheet is included. Table 2 provides a

description of the key parameters that define each of these sets of samples. It should be noted that this report presents results for the samples with the smallest and largest thicknesses from each set, as the results for the intervening thicknesses follow consistent trends.

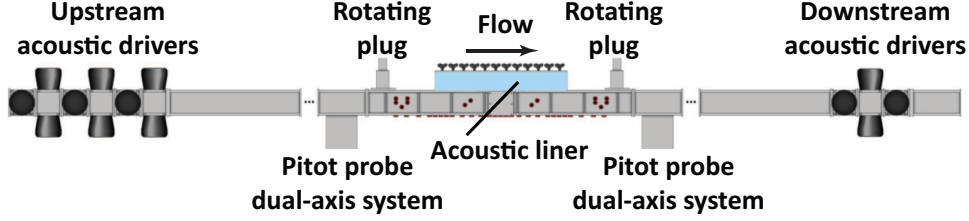


Figure 4: NASA Langley Grazing Flow Impedance Tube [Source: NASA].

Table 2: Test Liner Parameters.

Test Rig	NIT Set 1			NIT Set 2			GFIT Set 1		
Label	N1S1	N1S2	N1S3	N2S1	N2S2	N2S3	G1S1	G1S2	G1S3
$h$ (in)	1.500	1.500	1.500	1.504	1.504	1.504	1.503	1.503	1.503
$t_p$ (in)	0.009	0.024	0.038	0.096	0.146	0.195	0.098	0.147	0.195
$l_s$ (in)	0.391	0.376	0.362	0.304	0.254	0.205	0.302	0.253	0.205
$t$ (in)	-	-	-	0.037	0.037	0.037	0.038	0.038	0.038
$d$ (in)	-	-	-	0.018	0.018	0.018	0.017	0.017	0.017
$\sigma_a$	-	-	-	0.069	0.099	0.151	0.062	0.089	0.135
$\theta_f$	0.65	0.65	0.65	-	-	-	-	-	-

In the following, comparisons will be made between impedance spectra predicted using two distinct approaches. These two approaches are described with the aid of Figures 5 and 6. As indicated in Figure 5a, each test liner consists of a core that contains a  $5 \times 5$  array of square chambers with side length  $l_s$  and height  $h$ . A dotted black line is used to highlight the surface area of the opening for one of these chambers. In order to determine the surface impedance for a representative unit of the liner, the surface area needs to grow to include one-half of a partition thickness on all four boundaries of the chamber. This is depicted via the solid black line. Figure 5b provides a side view of one row of chambers, with the same dotted and solid black lines used to depict the two cross sectional areas of interest. A dashed red line is added to represent the inclusion of a facesheet. The surface impedance of the entire liner is expected to be identical to that predicted for a single unit cell (chamber plus partial partitions) since all chambers in these liners are identical.

The computational process consists of marching through the chamber from the backplate (station 0) to the surface of the facesheet (station  $3_{bf}$ ). Figure 6 provides two sketches of this representative chamber. Figure 6a contains a pictorial representation of one computational process that is considered in this investigation, namely to (1) compute the sound transmission through the core, (2) add the effects of blockage, and (3) add the effects of the facesheet. Figure 6b provides a corresponding pictorial representation of an alternate computational ordering, i.e., (1) compute the sound transmission through the core, (2) add the effects of the facesheet, and (3) add the effects of blockage (station 0 to station  $3_{fb}$ ). The key difference in these two computational approaches

is the amount of surface area that is included in the computation at each station. The subscripts 'bf' and 'fb' are used to denote whether the first or second computational approach is being used. The surface areas at stations 0, 1, and  $2_{fb}$  are given by  $A_a = (l_s)^2$  and the corresponding areas at stations  $2_{bf}$ ,  $3_{fb}$ , and  $3_{bf}$  are  $A_t = (l_s + t_p)^2$ .

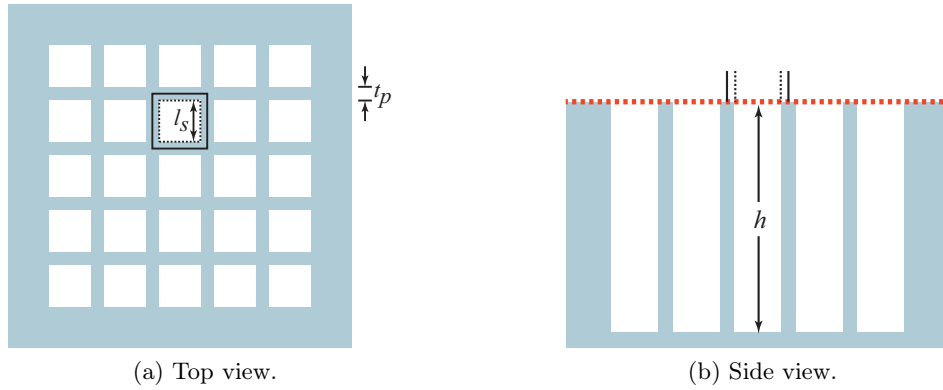


Figure 5: Sketch of representative liner. Solid and dotted black lines depict edges of active and total surfaces for a unit cell. Dashed red line depicts a facesheet (if present) [Source: NASA].

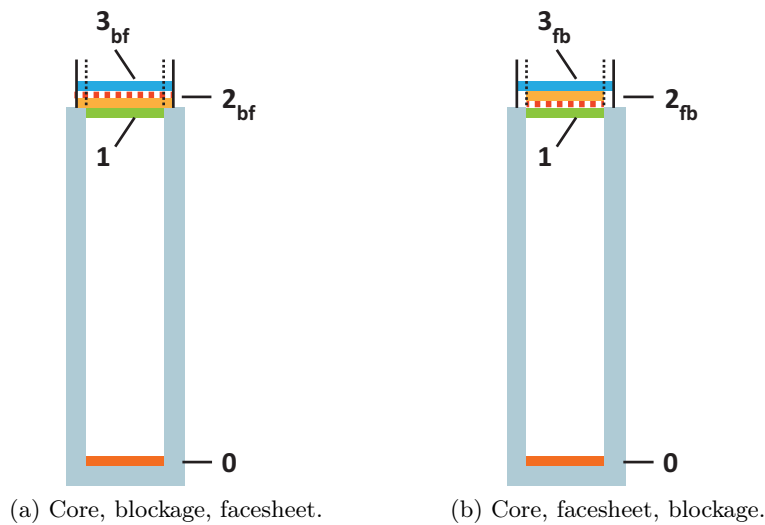


Figure 6: Sketches of representative chamber with two computational orders. Colored boxes represent measurement stations in the transmission line calculation. Dotted and solid black lines depict edges of active and total surfaces for a single chamber. Dashed red line depicts a facesheet (if present) [Source: NASA].

### 3 Liner Type 1 (uniform core, no facesheet)

The eventual goal is to apply improved modeling practices to design acoustic liners with complex core geometries. Initial validation tests with these novel configurations are often conducted in two stages, first with no facesheet and then with a wire mesh facesheet. This approach provides confirmation that the core has been built properly and then offers a very simple method to confirm that inclusion of a facesheet can be properly predicted. Wire mesh material is known to be quite linear (e.g., the material used in this study has a nonlinearity factor  $< 1.2$ ), such that the effects of SPL should be minimal.

The current study employs this approach with uniform-depth liners. The first set of results use data acquired with NIT Set 1 samples. It is well understood that the surface impedance for a uniform-height core with no facesheet can be estimated as  $\zeta_s = -\cot(kh)$  if the partition thickness,  $t_p$ , is negligible and the cross section of each core chamber is sufficiently large (e.g., conventional phenolic honeycomb core). For this case, the only resistance contribution is due to the viscothermal losses along the partition surfaces, which is virtually negligible. However, this simplified prediction does not explicitly account for the inclusion of thicker partitions. Thus, the ZKTL model [7–9] is used to predict the surface impedance spectra for this set of samples.

Each calculation begins at station 0 (see Fig. 6). The normalized acoustic pressure,  $p_0$ , and particle velocity,  $u_0$ , at this station are assumed to be unity and zero, respectively.<sup>1</sup> The ZKTL model computes changes in acoustic pressure and particle velocity between stations 0 and 1 as

$$\begin{pmatrix} p_1 \\ u_1 \end{pmatrix} = \begin{pmatrix} \cosh(k\Gamma h) & \zeta_c \sinh(k\Gamma h) \\ \zeta_c^{-1} \sinh(k\Gamma h) & \cosh(k\Gamma h) \end{pmatrix} \begin{pmatrix} p_0 \\ u_0 \end{pmatrix}. \quad (1)$$

This analysis is based on transmission line theory provided by Zwikker and Kosten [10]. All acoustic pressures and particle velocities are normalized by  $\rho c^2$  and  $c$ , respectively, where the density of the air and the speed of sound are for the prevailing static pressure and air temperature. Also, impedances are assumed to be normalized by the characteristic impedance of air,  $\rho c$ , and an  $e^{i\omega t}$  time convention is used. The propagation constant,  $\Gamma$ , and characteristic impedance,  $\zeta_c$ , within the empty chamber are computed as

$$\Gamma = \sqrt{\frac{J_0(i^{3/2}s)}{J_2(i^{3/2}s)}} \sqrt{\frac{\gamma}{n_\Gamma}} \quad \text{and} \quad \zeta_c = \frac{-i J_0(i^{3/2}s)}{\Gamma J_2(i^{3/2}s)}. \quad (2)$$

where

$$s = (d_c/2) \sqrt{\rho_s \omega / \mu} \quad \text{and} \quad n_\Gamma = \left[ 1 + \frac{\gamma - 1}{\gamma} \frac{J_2(i^{3/2} P_n^{1/2} s)}{J_0(i^{3/2} P_n^{1/2} s)} \right]^{-1}. \quad (3)$$

If the partition thickness is negligible, the normalized acoustic impedance,  $\zeta_s$ , at the surface of the liner is equivalent to the normalized acoustic impedance at the surface of a single chamber, and is given by

$$\zeta_s = \zeta_1 = \frac{p_1}{u_1}. \quad (4)$$

---

<sup>1</sup>This choice for the acoustic pressure is chosen for convenience, as the linear version of the model depends only on the change in acoustic pressure between stations 0 and  $3_{bf}$  or between stations 0 and  $3_{fb}$ .

However, if the partition thickness is more substantial, the effects of blockage caused by these partitions is included via

$$\zeta_s = \zeta_{2_{bf}} = \zeta_1 \frac{A_t}{A_a}. \quad (5)$$

Examples of this blockage effect are illustrated in Figures 7 and 8, which provide comparisons of predicted and measured impedance spectra for two liner configurations (N1S1 and N1S3) with partition thicknesses of 0.009" and 0.038", respectively.

Observe the very small vertical scale for Figures 7a and 8a that is required to highlight the very slight differences between predicted and measured impedance spectra. Also, differences between predicted and measured reactance spectra are imperceptible. The effects of SPL are negligible, as should be expected for this type of liner. These results confirm that Equation (5) provides a good prediction of the surface impedance for uniform-depth liners with different partition thicknesses.

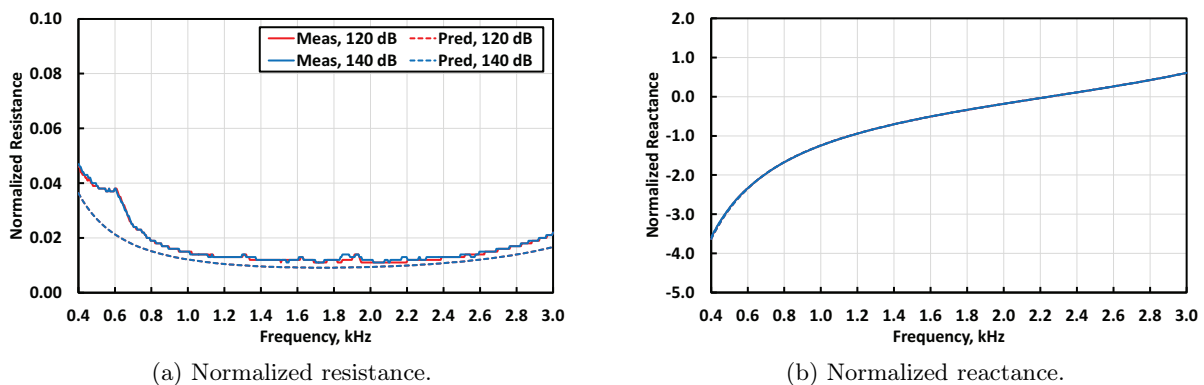


Figure 7: Predicted and measured impedances for sample N1S1 ( $t_p = 0.009''$ ).

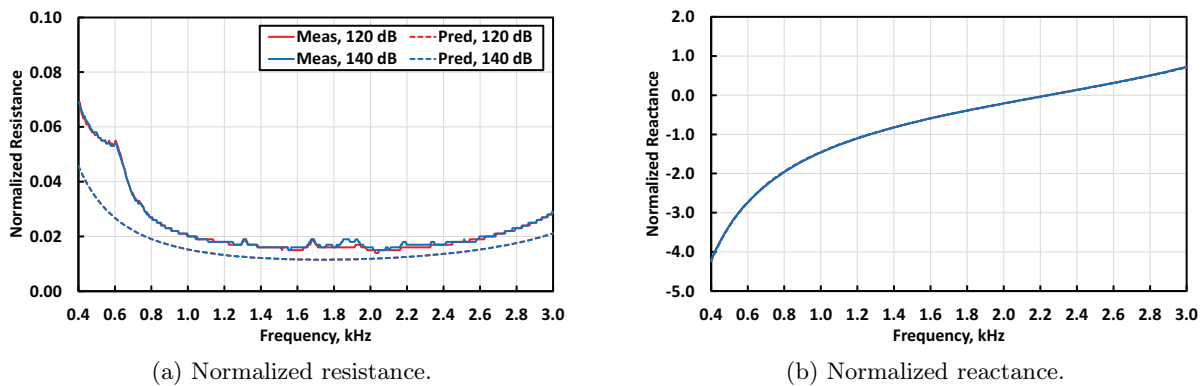


Figure 8: Predicted and measured impedances for sample N1S3 ( $t_p = 0.038''$ ).

## 4 Liner Type 2 (uniform core, wire mesh facesheet)

As noted earlier, the next step toward improved model validation is to explore the addition of a wire mesh facesheet. A uniform liner with negligible partition thickness and a wire mesh facesheet

is often approximated using the very simple relation  $\zeta_s = \theta_f - i \cot(kh)$ , where  $\theta_f$  is the normalized DC flow resistance of the wire mesh. This liner type is studied with a combination of NIT Set 1 cores and a wire mesh facesheet.

For complex cores (e.g., a combination of chambers with different heights), it is often of interest to evaluate the effects of adding a wire mesh facesheet. This type of material is known to be quite linear (e.g., the material used in this study has a nonlinearity factor  $< 1.2$ ), such that the effects of SPL should be minimal.

If we continue with the transmission line calculations, the surface impedance for a wire mesh over the uniform-height core with negligible partition thickness builds upon Equation (1) via

$$\begin{pmatrix} p_{2_{fb}} \\ u_{2_{fb}} \end{pmatrix} = \begin{pmatrix} 1 & \theta_f \\ 0 & 1 \end{pmatrix} \begin{pmatrix} p_1 \\ u_1 \end{pmatrix}. \quad (6)$$

The resultant acoustic pressure,  $p_{2_{fb}}$ , and particle velocity,  $u_{2_{fb}}$ , are then used to compute the surface impedance at station  $2_{fb}$ ,<sup>2</sup>

$$\zeta_s = \zeta_{2_{fb}} = \frac{p_{2_{fb}}}{u_{2_{fb}}}. \quad (7)$$

However, if the partition thickness becomes more substantial, the surface impedance is modified by the inclusion of these rigid wall surfaces. There are at least two methods to include these effects in the analysis. The first is to apply blockage effects to the empty core result,  $\zeta_1$ , before adding the effects of the wire mesh. This can be achieved with simple modifications to Equations (4) and (6). First, the effects of blockage on the acoustic pressure and particle velocity at the upper surface of the empty core are computed as

$$\begin{pmatrix} p_{2_{bf}} \\ u_{2_{bf}} \end{pmatrix} = \begin{pmatrix} p_1 A_t / A_a \\ u_1 A_a / A_t \end{pmatrix}, \quad (8)$$

where the  $a$  and  $t$  subscripts are used to depict the locations inside the solid and dotted squares, respectively, of Figure 5. The effects of the wire mesh are then added via

$$\begin{pmatrix} p_{3_{bf}} \\ u_{3_{bf}} \end{pmatrix} = \begin{pmatrix} 1 & \theta_f \\ 0 & 1 \end{pmatrix} \begin{pmatrix} p_{2_{bf}} \\ u_{2_{bf}} \end{pmatrix}, \quad (9)$$

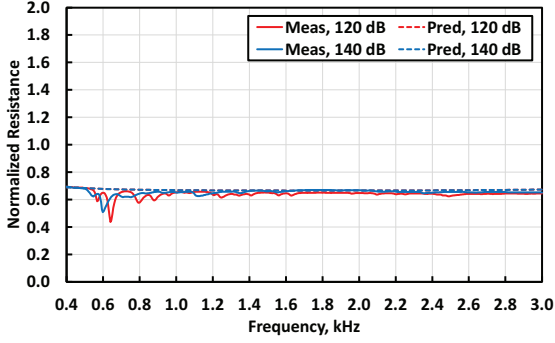
and the surface impedance can be computed via

$$\zeta_s = \zeta_{3_{bf}} = \frac{p_{3_{bf}}}{u_{3_{bf}}}. \quad (10)$$

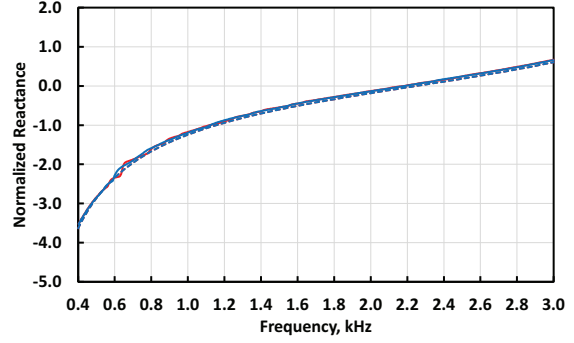
Figures 9 and 10 present impedance spectra for two liners (N1S1 and N1S3) with a wire mesh facesheet, for which the predicted impedances have been computed using this formulation [Eqs. (1, 8, 9, and 10)]. The comparison of predicted and measured resistance spectra is quite good and the corresponding comparison for the reactance component is excellent. As expected, the effects of SPL are minimal.

---

<sup>2</sup>Note that stations  $2_{fb}$  and  $2_{bf}$  are identical when the partition thickness is negligible.



(a) Normalized resistance.

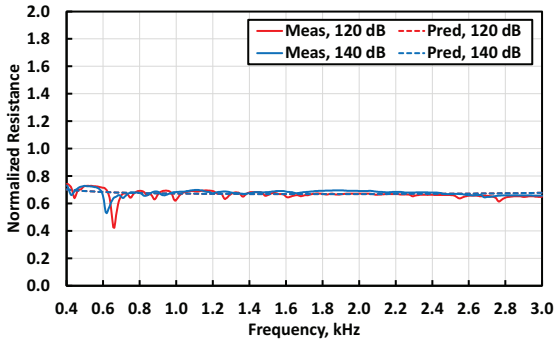


(b) Normalized reactance.

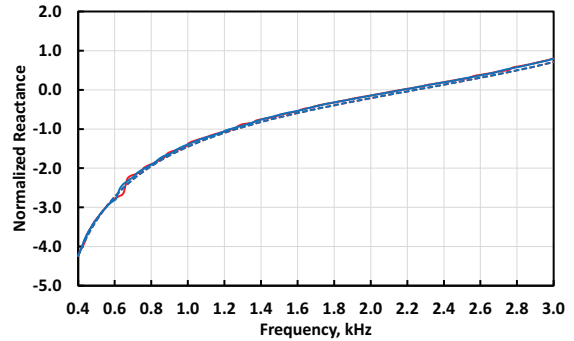
Figure 9: Predicted and measured impedances for sample N1S1 with wire mesh facesheet ( $t_p = 0.009''$ ). Computational order: core, add blockage, add mesh.

Another approach to account for partition thickness effects is to first add the effects of the wire mesh, and then to include the effects of blockage to achieve a surface impedance. This approach begins by computing the impedance,  $\zeta_{2_{fb}}$  [Eq. (7)], at the upper surface of the portion of wire mesh that is over the empty chamber. Blockage effects are then added via

$$\zeta_s = \zeta_{3_{fb}} = \zeta_{2_{fb}} \frac{A_t}{A_a}. \quad (11)$$



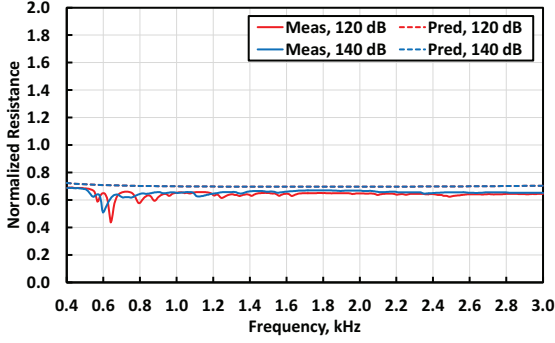
(a) Normalized resistance.



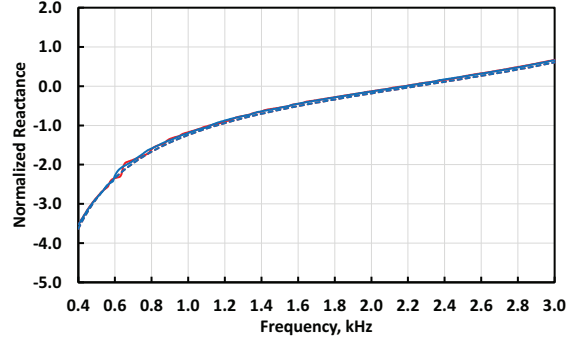
(b) Normalized reactance.

Figure 10: Predicted and measured impedances for sample N1S3 with wire mesh facesheet ( $t_p = 0.038''$ ). Computational order: core, add blockage, add mesh.

Figures 11 and 12 present results for the same two configurations (N1S1 and N1S3 with a wire mesh facesheet), where the predictions have been generated using this second approach [Eqs. (1, 6, 7, and 11)]. While the reactance spectra comparisons remain excellent, this method results in a noticeable overprediction of the measured resistance spectrum.

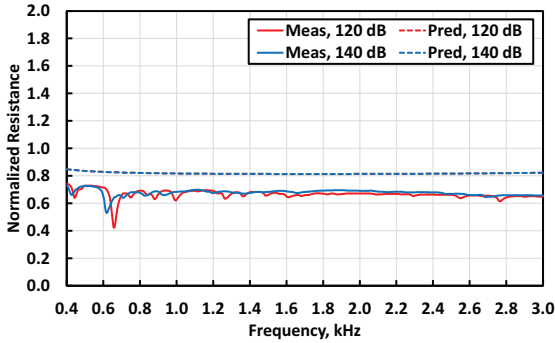


(a) Normalized resistance.

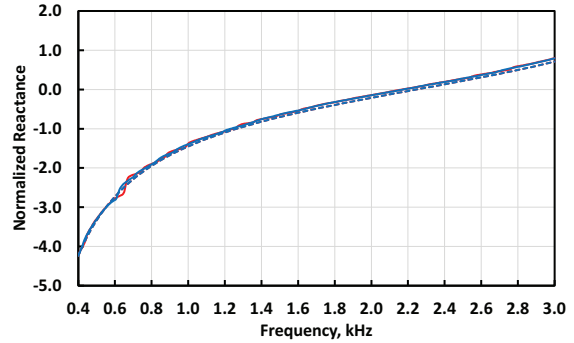


(b) Normalized reactance.

Figure 11: Predicted and measured impedances for sample N1S1 with wire mesh facesheet ( $t_p = 0.009''$ ). Computational order: core, add mesh, add blockage.



(a) Normalized resistance.



(b) Normalized reactance.

Figure 12: Predicted and measured impedances for sample N1S3 with wire mesh facesheet ( $t_p = 0.038''$ ). Computational order: core, add mesh, add blockage.

Based on these results, the first approach (compute core impedance, add blockage effects, add mesh) provides superior results for liners with partition thicknesses up to  $0.038''$ , whereas resistance spectra predicted with the second approach deviate from the measured results for partitions as thin as  $0.009''$ .

## 5 Liner Type 3 (uniform core, perforated facesheet)

The third type of liner is generally of greater interest to the liner community, as it is the most common configuration and is suitable for flight applications. This liner type contains a perforated facesheet mounted over the uniform core. With current AM printers, a perforated facesheet can be integrated with the core such that there is no gap between them. When manufactured this way, the perforations in the facesheet can be positioned such that they are over the active (open) portion of the core, i.e., none of the perforations are over the solid partitions. However, perforated facesheets add more nonlinearity to the design process, such that the results are dependent on SPL (and Mach

number if there is flow over the liner surface). There are many models to incorporate the effects of a perforated facesheet into the impedance prediction process [9].

Similar to that described above for Liner Type 2, two approaches are considered to incorporate the effects of partition thickness into the impedance prediction. The first assumes a computational order of (1) compute the impedance at the upper boundary of the core, (2) add blockage effects, and (3) add the effects of the perforated facesheet. Alternatively, the second approach reverses the order of these last two steps. Each approach is explored using two sets of liners, NIT Set 2 and GFIT Set 1.

There are a number of distinctions between NIT and GFIT tests. The most obvious one is the angle of incidence. Sound impinges at normal incidence in the NIT, but passes over the liner tangentially in the GFIT. The GFIT supports the addition of mean flow as well, but that effect is not included in the present study. The entirety of an NIT sample surface is exposed to the same SPL, whereas the level is constantly changing over the surface of a GFIT sample. The NIT only supports propagation of plane waves over the frequency range of interest but a liner placed in the GFIT will be exposed to multiple soft-wall modes. Finally, the methods used for educing the impedance of samples in the NIT and GFIT are quite different.

## 5.1 NIT Set 2 Results

The first process begins with computation [Eq. (1)] of the acoustic pressure and particle velocity at the upper boundary of the empty chamber. Equation (8) is then applied to transition from station 1 to station  $2_{\text{bf}}$ , resulting in the impedance given by  $\zeta_{2_{\text{bf}}}$ . The impedance over this full surface is then computed using a slightly modified version<sup>3</sup> of the perforated facesheet impedance prediction model presented by Motsinger and Kraft [11]. This is given by

$$\zeta_s = \zeta_{3_{\text{bf}}} = \frac{a\mu t}{2\rho c(\sigma C_D)d^2} + \frac{\kappa_i + \kappa_e}{2c(\sigma C_D)}v_{\text{rms}} + \theta_{\text{gf}} + i \left\{ \frac{k(t + \epsilon d)}{\sigma} + \zeta_{2_{\text{bf}}} \right\}, \quad (12)$$

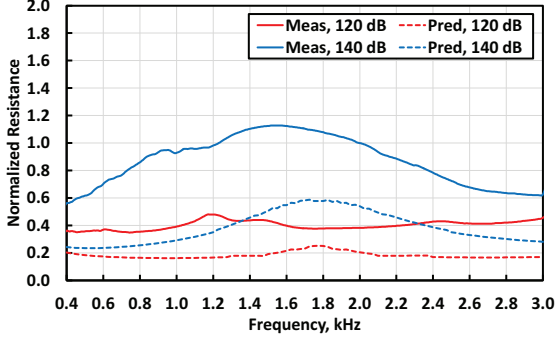
where

$$\epsilon = \frac{0.85(1 - 0.7\sqrt{\sigma})}{1 + 305M_{C/L}^3} \quad \text{and} \quad \theta_{\text{gf}} = \frac{M_{C/L}}{\sigma \{2 + 1.256 (\delta_1/d)\}}. \quad (13)$$

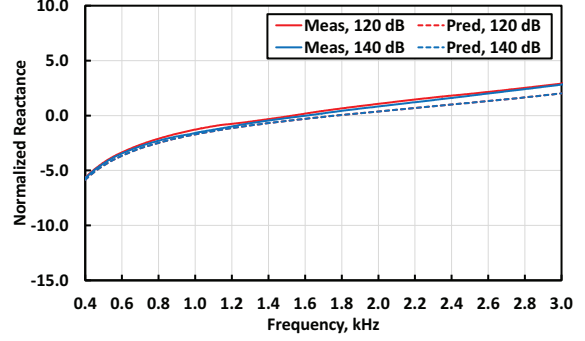
Figures 13 and 14 present results using this approach for two NIT samples (N2S1 and N2S3) with a perforated facesheet. The predicted and measured reactance spectra compare favorably for sample N2S1 ( $t_p = 0.096''$ ), with a slight divergence at the higher frequencies. However, the measured resistance spectra are significantly underpredicted for this sample over the entire frequency range of interest. These comparisons diverge further as the partition thickness is increased (sample N2S3,  $t_p = 0.195''$ ).

---

<sup>3</sup>The standard version of the model assumes the core impedance, shown as  $\zeta_{2_{\text{bf}}}$  in Equation (12), is given as  $-i \cot(kh)$ .

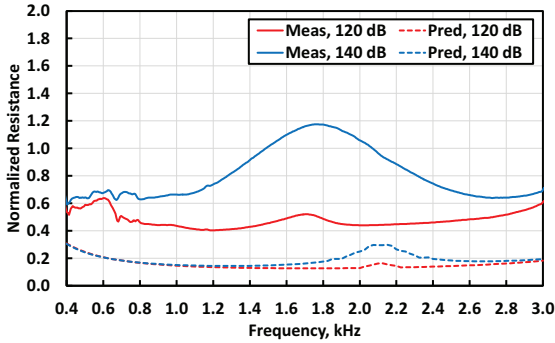


(a) Normalized resistance.

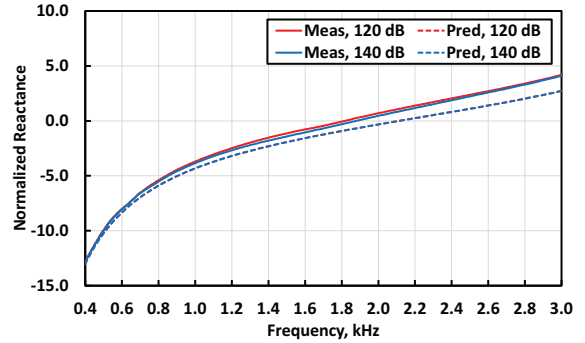


(b) Normalized reactance.

Figure 13: Predicted and measured impedances for sample N2S1 with perforated facesheet ( $t_p = 0.096''$ ). Computational order: core, add blockage, add perforate.



(a) Normalized resistance.



(b) Normalized reactance.

Figure 14: Predicted and measured impedances for sample N2S3 with perforated facesheet ( $t_p = 0.195''$ ). Computational order: core, add blockage, add perforate.

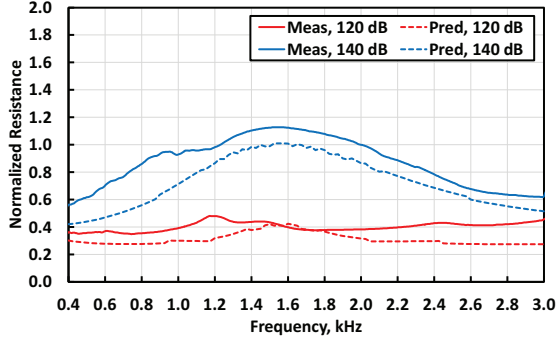
The second process starts with computation of the impedance,  $\zeta_1$ , at the upper boundary of the chamber (station 1). The effects of the perforated facesheet are added via Equations (12 and 13), with one exception. The  $\zeta_{2_{bf}}$  term, which captures the core effects in Equation (12), is replaced by  $\zeta_1$ , i.e.,

$$\zeta_{2_{fb}} = \frac{a\mu t}{2\rho c(\sigma C_D)d^2} + \frac{\kappa_i + \kappa_e}{2c(\sigma C_D)}v_{\text{rms}} + \theta_{gf} + i \left\{ \frac{k(t + \epsilon d)}{\sigma} + \zeta_1 \right\}. \quad (14)$$

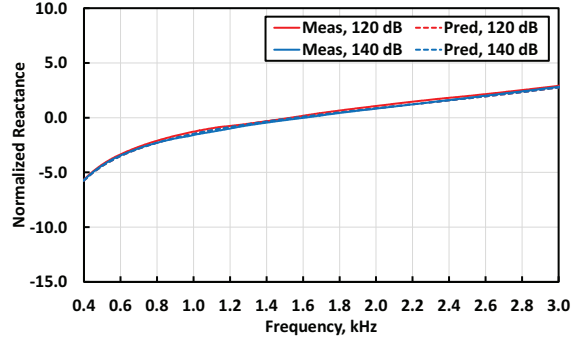
Blockage effects are then added to determine the surface impedance via

$$\zeta_s = \zeta_{3_{fb}} = \zeta_{2_{fb}} \frac{A_t}{A_a}. \quad (15)$$

Figures 15 and 16 present results using this second approach for the same two NIT samples (N2S1 and N2S3). The resistance comparison is significantly better than that observed with the first approach, while the reactance comparison is excellent over the entire frequency range. The effects of partition thickness appear to be well captured by this second approach.

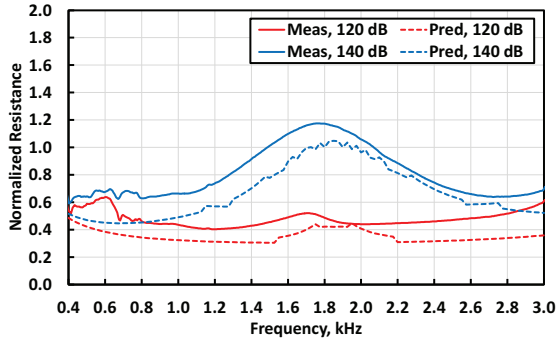


(a) Normalized resistance.

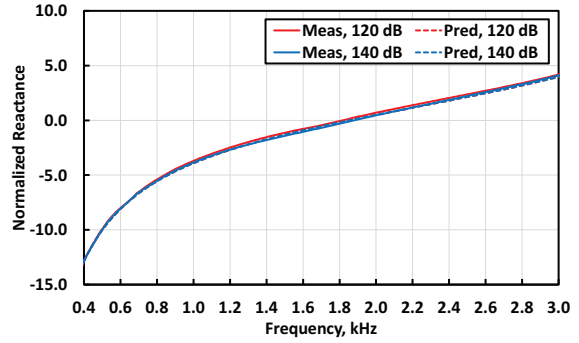


(b) Normalized reactance.

Figure 15: Predicted and measured impedances for sample N2S1 with perforated facesheet ( $t_p = 0.096''$ ). Computational order: core, add perforate, add blockage.



(a) Normalized resistance.



(b) Normalized reactance.

Figure 16: Predicted and measured impedances for sample N2S3 with perforated facesheet ( $l_p = 0.195''$ ). Computational order: core, add perforate, add blockage.

## 5.2 GFIT Set 1 Results

Data were also acquired with two GFIT samples (G1S1 and G1S3) with geometry parameters similar to those tested in the NIT. The NIT results provide evidence that it is important to include the perforated facesheet effects prior to accounting for the surface blockage due to partition thickness. The following results explore the extension of this to data acquired in the GFIT.

Figures 17 and 18 present comparisons of predicted and measured impedance spectra for the G1S1 ( $t_p = 0.098''$ ) sample, where the predictions were computed using each approach. The predicted resistance spectra follow a similar trend to that observed with the measured results, with a gradual increase in magnitude with increasing SPL. The resistance spectra computed using the first approach (computational order: core, add blockage, add perforate) compare favorably with the measured results, especially for the middle frequency range (nominally 1.0 to 2.0 kHz). The corresponding resistance spectra computed using the second approach (computational order: core, add perforate, add blockage) diverge from the measured results in this middle frequency range, but converge to the measured results at frequencies nearer the upper and lower limits (i.e., for frequen-

cies farther away from resonance). Comparisons between predicted and measured reactance spectra are very favorable for both computational approaches.

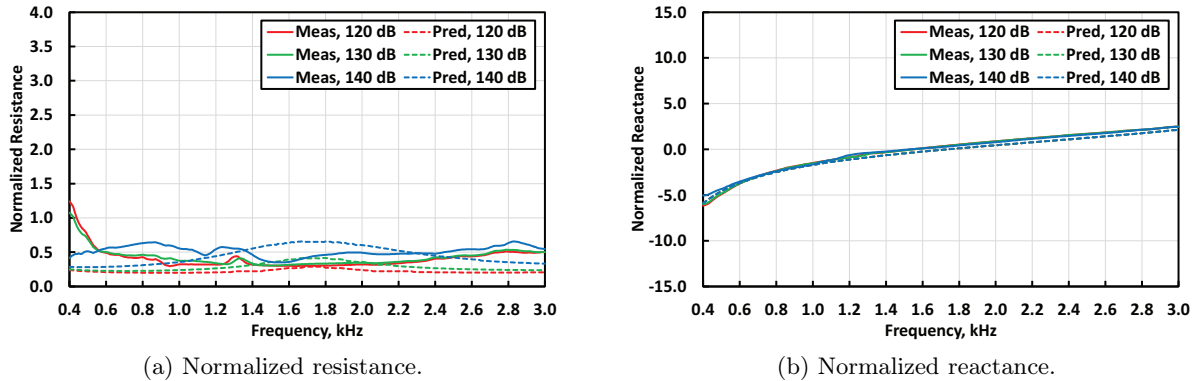


Figure 17: Predicted and measured impedances for sample G1S1 with perforated facesheet ( $t_p = 0.098$ ). Computational order: core, add blockage, add perforate.

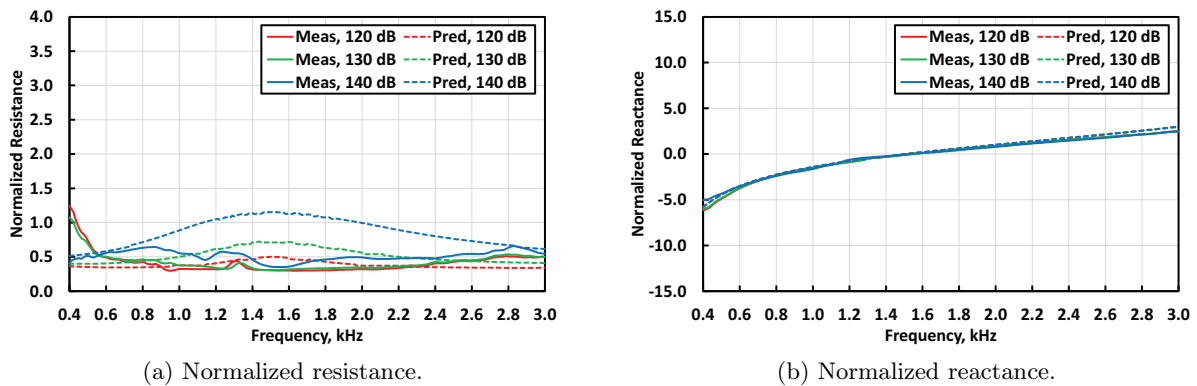
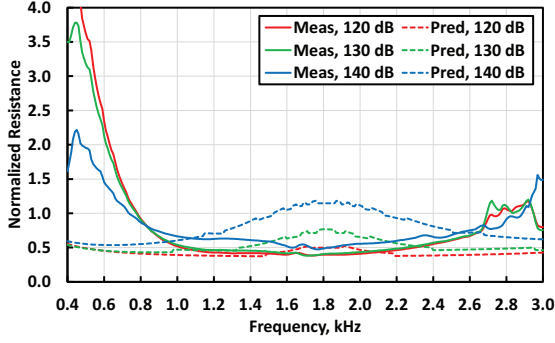
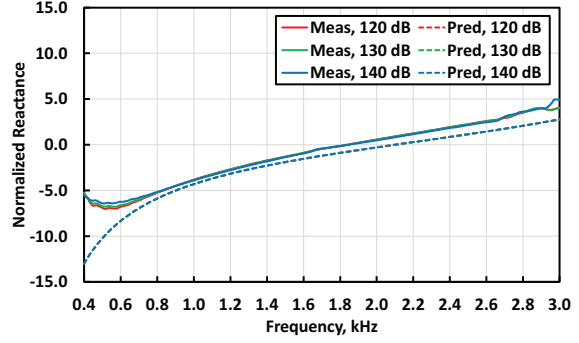


Figure 18: Predicted and measured impedances for sample G1S1 with perforated facesheet ( $t_p = 0.098$ ). Computational order: core, add perforate, add blockage.

For the thicker partitions (sample G1S3,  $t_p = 0.195$ ), the resistance spectra comparisons (Figs. 19 and 20) with the first computational approach appear somewhat better than those achieved with the second approach. Conversely, the reactance spectra comparisons are acceptable with the first approach, but are much better with the second approach.

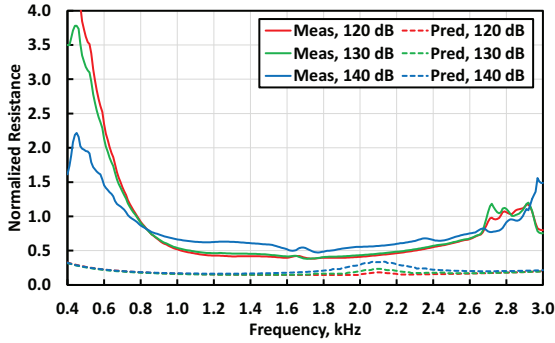


(a) Normalized resistance.

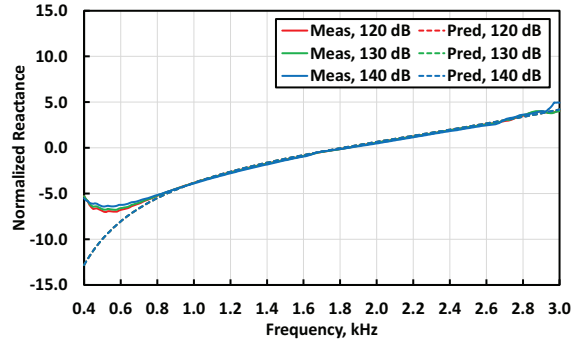


(b) Normalized reactance.

Figure 19: Predicted and measured impedances for sample G1S3 with perforated facesheet ( $t_p = 0.195$ ). Computational order: core, add blockage, add perforate.



(a) Normalized resistance.



(b) Normalized reactance.

Figure 20: Predicted and measured impedances for sample G1S3 with perforated facesheet ( $t_p = 0.195$ ). Computational order: core, add perforate, add blockage.

It is interesting to note the differences between results measured in the NIT and GFIT. The NIT results strongly suggest that it is better to include the effects of the perforated facesheet before accounting for the effects of blockage, while the GFIT results would seem to suggest that including the effects of blockage before accounting for the perforated facesheet might be better. However, it is important to note that the impedance prediction model does not fully account for nonlinear effects of the perforated facesheet. This is the subject of a separate investigation that is currently being conducted. Also, the prediction model assumes the entire surface of the liner is exposed to the same SPL. This is clearly true for tests conducted in the NIT with a plane-wave source, while it is certainly violated for tests in the GFIT. Specifically, the SPL reported for the data measured in the GFIT is the level achieved at the leading edge of the liner. Sound attenuation over the length of the liner can become significant for frequencies near resonance (around 1.8 kHz for these liners), which means the average SPL to which the liner is exposed may be quite different. Each of these effects (and possibly others) are intended to be the focus of further investigation. For now, it is the authors' view that the preferred approach is that observed with the NIT data, which suggests that the effects of the perforated facesheet should be included prior to accounting for the effects of blockage.

## 6 Summary of Partition Thickness Effects on Impedance Modeling

Three types of uniform-depth liners were considered in the current study, each containing a  $5 \times 5$  array of square chambers. If the partition thickness is negligible, the surface impedance of the entire liner is equivalent to the surface impedance of a single chamber, which can be predicted using a model based on transmission line theory provided by Zwikker and Kosten. If the partition thickness becomes more substantial, the unit cell in the impedance calculation extends beyond the active surface (i.e., the opening) to include one-half of the partition thickness around the perimeter of the chamber. For this case, it is generally assumed that the surface impedance of the entire liner can be reasonably approximated by the effective impedance of this unit cell. For liners with no facesheet (Liner Type 1), the change in impedance between the upper boundary of the open chamber and the full surface that includes one-half of the partition thickness around the perimeter of the chamber is predicted to be a function of the change in cross sectional area. Results attained with this set of samples mounted in the NIT confirm that this holds true.

The second group of liner configurations (Liner Type 2) consisted of a wire mesh facesheet mounted onto the same set of uniform-depth cores. Two approaches were considered for the prediction of the surface impedance over the unit cell that includes the partial partition thickness. The first assumes the effects of blockage should be incorporated (for the active chamber) prior to accounting for the effects of adding the wire mesh. The second assumes the transfer impedance across the wire mesh should be considered before the effects of blockage due to the partition thickness are incorporated. Results for this set of NIT liners suggest the first approach is preferred. It is believed that this may be due to the fact that the transfer impedance across the wire mesh is computed using a lumped element model.

Additional NIT liners (Liner Type 3) were built that used slightly different partition thicknesses and contained a perforated facesheet instead of a wire mesh. The same two approaches were considered to account for the effects of partition thickness on the predicted surface impedance. In contrast to the model used for the wire mesh, the Motsinger and Kraft model used to include the effects of the perforated facesheet explicitly includes the effects of the core. This integrated modeling is believed to be key to the observation that the second approach (incorporate effects of perforate before accounting for the effects of the partition thickness) provides predicted impedance spectra that are much closer to the measured results.

A set of GFIT liners with the same geometric features (Liner Type 3) was also considered. The data presented herein are confined to Mach 0.0 results. The results are not definitive, i.e., a portion of the results are aligned with those achieved with the NIT liners but other results are not. This is conjectured to be due to the differences between the ways in which the impedances are measured, in particular the different sound fields to which the liner is exposed in the two test rigs. Detailed study of this phenomenon and the effects of tangential mean flow is intended to be the focus of a future investigation. For now, it is believed best to proceed using the NIT results as a guide, i.e., incorporate perforate effects before accounting for partition thickness.

## Acknowledgements

This work was funded by the Advanced Air Transport Technology Project of the NASA Advanced Air Vehicles Program. The authors wish to express thanks to all members of the NASA Langley Liner Physics Team for their efforts in collecting the experimental data.

## References

1. Chung, J. Y. and Blaser, D. A., “Transfer Function Method of Measuring In-Duct Acoustic Properties: I. Theory,” *Journal of Acoustical Society of America*, Vol. 68, 1980, pp. 907–921.
2. Jones, M. G. and Stiede, P. E., “Comparison of Methods for Determining Specific Acoustic Impedance,” *Journal of the Acoustical Society of America*, Vol. 101, No. 5, May 1997, pp. 2694–2704.
3. Jones, M. G., Watson, W. R., Nark, D. M., Howerton, B. M., and Brown, M. C., “A Review of Acoustic Liner Experimental Characterization at NASA Langley,” NASA TP 220583, April 2020.
4. Howerton, B. M., Vold, H., and Jones, M. G., “Application of Sine Sweep Excitation for Acoustic Impedance Education,” AIAA Paper 2019-2487, May 2019.
5. de Prony, R., “Essai Éxperimental et Analytique: Sur Les Lois de la Dilatabilité de Fluides Élastique et sur Celles de la Force Expansive de la Vapeur de L’alkool, Àdifférentes Temperatures,” *Journal de l’école Polytechnique*, Vol. 1, No. 22, 1795, pp. 24–76.
6. Watson, W. R., Carpenter, M. H., and Jones, M. G., “Performance of Kumaresan and Tufts Algorithm in Liner Impedance Education with Flow,” *AIAA Journal*, Vol. 53, No. 4, April 2015, pp. 1091–1102.
7. Parrott, T. L. and Jones, M. G., “Parallel-Element Liner Impedances for Improved Absorption of Broadband Sound in Ducts,” *Noise Control Engineering Journal*, Vol. 43, No. 6, Nov. 1995.
8. Jones, M. G., Howerton, B. M., and Ayle, E., “Evaluation of Parallel-Element, Variable-Impedance, Broadband Acoustic Liner Concepts,” AIAA Paper 2012-2194, June 2012.
9. Jones, M. G. and Nark, D. M., “Comparisons of Impedance Prediction Models for Perforate-Over-Honeycomb Liners,” AIAA Paper 2023-3637, June 2023.
10. Zwicker, C. and Kosten, C., *Sound Absorbing Materials*, Elsevier Publishing Company, 1949.
11. Motsinger, R. E. and Kraft, R. E., “Design and Performance of Duct Acoustic Treatment: Aeroacoustics of Flight Vehicles; Chapter 14, Vol. 2: Noise Control,” NASA RP 1258, Aug. 1991.



**REPORT DOCUMENTATION PAGE**

*Form Approved*  
OMB No. 0704-0188

The public reporting burden for this collection of information is estimated to average 1 hour per response, including the time for reviewing instructions, searching existing data sources, gathering and maintaining the data needed, and completing and reviewing the collection of information. Send comments regarding this burden estimate or any other aspect of this collection of information, including suggestions for reducing this burden, to Department of Defense, Washington Headquarters Services, Directorate for Information Operations and Reports (0704-0188), 1215 Jefferson Davis Highway, Suite 1204, Arlington, VA 22202-4302. Respondents should be aware that notwithstanding any other provision of law, no person shall be subject to any penalty for failing to comply with a collection of information if it does not display a currently valid OMB control number.  
**PLEASE DO NOT RETURN YOUR FORM TO THE ABOVE ADDRESS.**

<b>1. REPORT DATE (DD-MM-YYYY)</b> 01-09-2023		<b>2. REPORT TYPE</b> Technical Memorandum		<b>3. DATES COVERED (From - To)</b>	
<b>4. TITLE AND SUBTITLE</b> Partition Thickness Considerations for Additively Manufactured Acoustic Liners				<b>5a. CONTRACT NUMBER</b>	
				<b>5b. GRANT NUMBER</b>	
				<b>5c. PROGRAM ELEMENT NUMBER</b>	
<b>6. AUTHOR(S)</b> M. G. Jones and D. M. Nark NASA Langley Research Center, Hampton, VA 23681				<b>5d. PROJECT NUMBER</b>	
				<b>5e. TASK NUMBER</b>	
				<b>5f. WORK UNIT NUMBER</b>	
<b>7. PERFORMING ORGANIZATION NAME(S) AND ADDRESS(ES)</b> NASA Langley Research Center Hampton, Virginia 23681-2199				<b>8. PERFORMING ORGANIZATION REPORT NUMBER</b>	
<b>9. SPONSORING/MONITORING AGENCY NAME(S) AND ADDRESS(ES)</b> National Aeronautics and Space Administration Washington, DC 20546-0001				<b>10. SPONSOR/MONITOR'S ACRONYM(S)</b> NASA	
				<b>11. SPONSOR/MONITOR'S REPORT NUMBER(S)</b> NASA/TM-20230013028	
<b>12. DISTRIBUTION/AVAILABILITY STATEMENT</b> Unclassified-Unlimited Subject Category xx Availability: NASA STI Program (757) 864-9658					
<b>13. SUPPLEMENTARY NOTES</b>					
<b>14. ABSTRACT</b>					
<b>15. SUBJECT TERMS</b> liner, acoustic impedance					
<b>16. SECURITY CLASSIFICATION OF:</b>			<b>17. LIMITATION OF ABSTRACT</b>	<b>18. NUMBER OF PAGES</b>	<b>19a. NAME OF RESPONSIBLE PERSON</b>
<b>a. REPORT</b>	<b>b. ABSTRACT</b>	<b>c. THIS PAGE</b>			STI Information Desk (help@sti.nasa.gov)
U	U	U	UU	26	<b>19b. TELEPHONE NUMBER (Include area code)</b> (757) 864-9658



---